

A hybrid framework for assessing outdoor thermal comfort in large-scale urban environments



Siqi Jia ^{a,b,d}, Yuhong Wang ^e, Nyuk Hien Wong ^f, Qihao Weng ^{a,b,c,*}

^a JC STEM Lab of Earth Observations, Department of Land Surveying and Geo-Informatics, The Hong Kong Polytechnic University, Hung Hom, Hong Kong, China

^b Research Centre for Artificial Intelligence in Geomatics, The Hong Kong Polytechnic University, Hung Hom, Hong Kong, China

^c Research Institute for Land and Space, The Hong Kong Polytechnic University, Hung Hom, Hong Kong, China

^d Landscape Architecture, Department of Architecture, Faculty of Architecture, The University of Hong Kong, China

^e Department of Civil and Environmental Engineering, Faculty of Construction and Environment, The Hong Kong Polytechnic University, Hung Hom, Kowloon, Hong Kong, China

^f Department of Building, School of Design and Environment, National University of Singapore, 4 Architecture Drive, Singapore 117566, Singapore

HIGHLIGHTS

- Sky view factor shows the strongest correlation with outdoor thermal comfort.
- During hot summers, 74.8% of urban areas in Hong Kong experienced strong to extreme heat stress.
- Most individuals perceived slight cold stress to neutral during the coldest conditions of Hong Kong.
- High levels of thermal stress were noted in urban layouts with low-rise buildings.
- In both LCZs 3 and 6, over 90% of areas experienced strong to extreme thermal stress.

ARTICLE INFO

Keywords:
Outdoor thermal comfort
Radiant temperature
Local climate zone
Neural network model
Urban climate
Urban morphology

ABSTRACT

Given the challenges posed by rapid urbanization and global warming, outdoor thermal comfort has become crucial for urban livability. However, there is a lack of field survey-based research on large-scale thermal comfort assessment across continuous urban spaces. To address this gap, this study developed a framework for assessing outdoor thermal comfort. A total number of 668 onsite observations from field studies during the daytime on typical summer days were collected and used for model development. The sites were distributed in diverse local climate zones (LCZs) of Hong Kong, enabling the prediction of outdoor thermal comfort across the city under different urban settings. A neural network model was trained for predicting daytime outdoor thermal comfort based on both meteorological and morphological variables. Universal Thermal Climate Index (UTCI) was used to indicate objective measures of human thermal comfort. The model was then applied to wider urban layouts and dynamic climatic conditions. The results revealed that during extreme hot conditions, approximately 74.8% of areas experienced strong to extreme heat stress, with thermal sensations classified as hot or very hot, while the remaining 25.3% fell under moderate heat stress. High levels of thermal stress were observed in urban layouts of low-rise buildings, with LCZ 3 showing the highest extreme heat stress percentage at 61.3%, followed closely by LCZ 6 at 57.6%. In both LCZs, over 90% of areas faced strong to extreme thermal stress. These findings are crucial for identifying urban regions with high thermal stress. The framework could be valuable for cities with similar climate and geographical contexts.

1. Introduction

Over half of the world's population currently lives in urban areas. It is projected that the urban population ratio will rise 68 % by 2050 (Dye,

2008; UNDESA, 2018). This urbanization process has notably led to the urban heat island (UHI), a phenomenon characterized by higher air temperatures in urban settings than their rural counterparts (Oke, 1982). As pedestrians are directly exposed to a variety of outdoor

* Corresponding author at: Department of Land Surveying and Geo-Informatics, The Hong Kong Polytechnic University, 11 Yuk Choi Rd, Hung Hom, Hong Kong.
E-mail addresses: siqjia@hku.hk (S. Jia), yuhong.wang@polyu.edu.hk (Y. Wang), bdgwnh@nus.edu.sg (N.H. Wong), qihao.weng@polyu.edu.hk (Q. Weng).

thermal conditions, increased urban air temperature temperatures have a substantive impact on their health, comfort, and quality of life (Avashia et al., 2021; Chen & Ng, 2012).

In the past few decades, the significance of creating thermally comfortable outdoor spaces, which are frequently used by people, has been increasingly recognized (Deng et al., 2023; Kumar & Sharma, 2020; Yahia & Johansson, 2014). A growing number of thermal comfort studies have been conducted for various outdoor spaces in different climate regions. Two broad categories of methods for measuring and modeling thermal comfort have been identified: The first category involves subjective perception of the thermal environment from a thermos-physiological perspective, while the second category focuses on objective measurements obtained through in-situ investigations of climatic parameters that influence human thermal comfort. For the subjective perception category, questionnaires are commonly used to collect data from respondents regarding personal information (such as age, gender, clothing), thermal perception, preferences, acceptability, etc. (Vanos et al., 2021). Past studies have indicated that the human thermal perception (e.g., thermal sensation votes – TSVs, or thermal comfort votes – TCVs) in outdoor environments is strongly influenced by a wide range of physiological and psychological factors (Schweiker et al., 2018). For example, it is widely acknowledged that behavioral responses to thermal environment differ by gender, age, and types of activities (Huang et al., 2016). In addition, research has explored human thermal comfort across diverse climatic conditions (Ng & Cheng, 2012; Villadiego & Velay-Dabat, 2014; Yin et al., 2021), revealing significant fluctuations in thermal adaptation across different climates. It is also identified that the pedestrians' behaviors and activities before approaching the surveyed site can impact their thermal states as well (Jia et al., 2022; Schweiker et al., 2018). Such subjective data reflects the most accurate and direct perceptions of the temperature by human beings. Human thermal comfort states are closely related to the observed conditions obtained through meteorological measurements. The subjective measurement of thermal responses also contributes significantly to the determination of thermal comfort standards in outdoor environments (Lau et al., 2022).

On the other hand, objective measurement of thermal comfort has been widely used in evaluating different thermal conditions in outdoor spaces (Liu et al., 2020). Questionnaire surveys and environmental data monitoring are often employed together to assess a subjective and objective outdoor thermal comfort evaluation, respectively (Rossi et al., 2022). In general, there are four key climatic parameters that influence the outdoor thermal comfort, i.e., air temperature (T_a), mean radiant temperature (T_{mrt}), relative humidity (rH), and wind speed (V_a) (Höppe, 1999; Johansson et al., 2014; Mayer & Höppe, 1987). Except T_{mrt} , other parameters can be directly measured by in-situ sensors. Accurate estimation of T_{mrt} becomes a critical element in evaluating outdoor thermal comfort. T_{mrt} is defined as "the uniform temperature of an imaginary enclosure in which the radiant heat transfer from the human body is equal to the radiant heat transfer in the actual non-uniform enclosure" (Guo et al., 2020; Thorsson et al., 2007). T_{mrt} , reflecting the thermal radiation received by humans in their surrounding environment (Lindberg et al., 2016; Manavvi & Rajasekar, 2020), significantly affects thermal comfort. However, measuring T_{mrt} is a challenging task due to the complex interactions among various thermal radiation sources in the environment (Guo et al., 2020).

Among the commonly used T_{mrt} measurement methods, the integral radiation method has been widely acknowledged as the most accurate one (Thorsson et al., 2007; VDI, 1998; Walikewitz et al., 2015). This method involves measuring the flux densities of short-wave and long-wave radiation emitted from the entire three-dimensional environment (Höppe, 1992; Manavvi & Rajasekar, 2020). However, its application in conducting large-scale outdoor observations is often limited due to the high cost and complexity of the measurement setup. Another widely used method to obtain an estimate of T_{mrt} is the globe thermometer method (Guo et al., 2020). This method utilizes a black-globe

thermometer, which captures the convective and radiative heat exchange occurring in its vicinity. While this method is popular due to its simplicity (Bedford & Warner, 1934), it can be time-consuming to reach thermal equilibrium due to the continuously changing radiative flux and air velocity in outdoor settings (Banfi et al., 2022; Spagnolo & de Dear, 2003). Additionally, some simulation models have been developed to estimate T_{mrt} and universal thermal indices, e.g., Rayman, ENVI-met, and SOLWEIG (Du et al., 2021; Guo et al., 2020; Lau et al., 2016). However, the accuracy of these models is significantly influenced by complex urban settings (Du et al., 2021).

Existing research predominantly concentrates on micro-scale assessments of outdoor thermal comfort, focusing on one or a few urban locations with limited spatial coverage (Su et al., 2024; Yang et al., 2013; Yin et al., 2021). Consequently, there is a lack of investigations of large-scale thermal comfort assessment at the city scale. This study aims to bridge this gap by conducting a comprehensive assessment of outdoor thermal comfort across the entire urban areas of Hong Kong. To achieve this objective, extensive field studies were conducted to collect detailed micro-climatic parameters from 668 measurement sites across various urban settings in Hong Kong during the daytime on typical summer days. Utilizing both meteorological and morphological variables throughout the study area, a neural network model was trained to predict daytime outdoor thermal comfort. The findings of this research offer valuable insights to policymakers and urban planners, aiding them in identifying urban areas that experience high levels of thermal stress or discomfort, and enabling them to take necessary actions to improve the thermal environment by implementing effective heat mitigation strategies.

2. Methodology

2.1. Overview of the methodology

Fig. 1 shows the flowchart of the overall analytical procedures, which comprises two phases. The first phase involves the collection of outdoor thermal comfort observations through field studies, while the second phase focuses on the predictive model development utilizing onsite data for objective thermal comfort prediction.

The first phase involves field studies conducted across 668 urban sites in Hong Kong during typical summer days. The selected sites were chosen to represent a diverse range of morphologies. Onsite measurements were carried out for each site to collect meteorological parameters. Additionally, detailed location information, including latitude and longitude, was recorded for each site. This information enables the derivation of site geometry details such as shading patterns, land use patterns, and other environmental parameters, using open geospatial data and Geographic Information System (GIS) tools. More details about the field survey are included in **Sections 2.2 and 2.3**. In the second phase, the entire dataset collected from the field studies was divided into two subsets: a training dataset and a testing dataset. The neural network model was trained and tested using these datasets to identify the structure that yielded the highest accuracy in predicting outdoor thermal comfort. This selected structure was then applied to larger areas, resulting in the generation of pixel-based outdoor thermal comfort in the whole urban areas of Hong Kong. The methods for the thermal comfort prediction were introduced in **Section 2.4**, including the derivation of explanatory variables, the calculation of thermal comfort indices, and the development of the neural network models. Then, to facilitate the assessment of mitigation measures in various urban settings, the concept of Local Climate Zone (LCZ) was incorporated. LCZs are designed to describe landscapes with distinct thermal climates based on their surface properties (Bechtel et al., 2015). Additionally, the application of the predictive model was extended to different climatic conditions in Hong Kong, providing insights into the thermal comfort range of outdoor urban spaces, the city's resilience to extreme heat events, and identifying areas that may require additional measures to mitigate heat

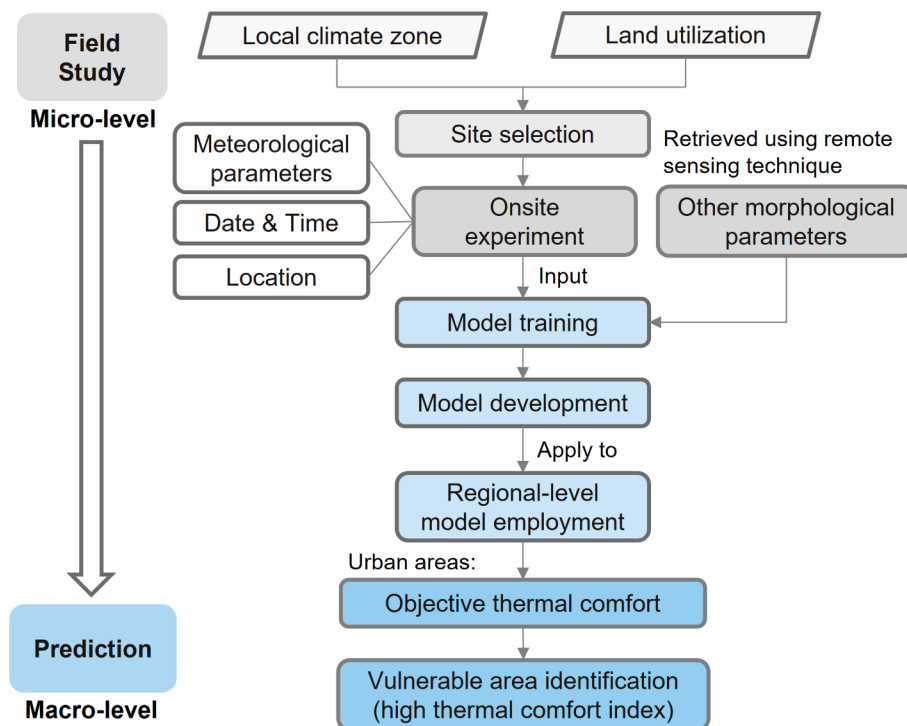


Fig. 1. Overview of the analytical procedures.

vulnerability.

2.2. Study area

Located on the southern coast of China, Hong Kong has a typical subtropical climate. The summer period in Hong Kong typically lasts from May to August, with sweltering temperatures and high humidity levels. According to the Hong Kong Observatory, there has been a consistent increasing trend in the annual mean temperature, with a rate of 0.3 °C per decade from 1994 to 2023. In 2023, the mean temperature for the summer months reached 29.7 °C, the highest on record. This persistent warming trend has become one significant threat for both the urban environment and residents in Hong Kong. As shown in Fig. 2, onsite observations were strategically distributed across 14 measurement zones of urban areas of Hong Kong.

The selection of measurement zones was guided by the LCZ classification system (Stewart & Oke, 2012; Wang et al., 2018) and Hong Kong land utilization (Plan.Dep., 2019). These zones included residential and commercial built-up areas with varying building densities and heights, urban canyons, and parks with different green space densities. The detailed locations of all survey points can be found in Supplementary Note 1. Based on these survey points, a neural network model was developed to predict daytime outdoor thermal comfort across the urban areas of Hong Kong. According to the LCZ classification (Stewart & Oke, 2012), LCZs 1–10 are defined as urban built-up types while LCZs A–G are classified as natural types. For this study, we selected LCZs 1 to 10 as the urban areas for applying the thermal comfort predictive model.

2.3. Field survey

The sensors used for the field survey include three net radiometers (Kipp & Zonen CNR4) and one weather station (Kestrel 5400 Heat Stress Tracker). The measured parameters include short-wave radiation (W/m^2), long-wave radiation (W/m^2), air temperature (°C), globe temperature (°C), relative humidity (%), and wind speed (m/s). Table 1 shows the sensors used for onsite measurements and the measurement

accuracy ranges for each sensor.

Onsite measurements were conducted during the daytime on cloudless summer days, specifically on July 22nd, 23rd, 26th, 28th, and 30th, 2021. These observations were made between 09:00 and 18:00. On each day, two to three measurement zones were surveyed. Within each measurement zone, a total of 42 to 53 observation sites were included. A total of 668 sites were surveyed during summer periods. Due to the extensive number of observations, we utilized a spot measurement approach, performed along a traverse within each measurement zone. The equipment was consistently stationed at a height of 1.5 m above the ground. Each site was observed for a duration of 3 min, with the specific date and time of each survey recorded, given that the sites were observed consecutively rather than concurrently. Throughout the survey duration, data was logged at 10-second intervals. The meteorological parameters gathered at each site were processed using a 3-minute average value.

2.4. Methods for predicting the outdoor thermal comfort

2.4.1. Explanatory variables

Based on previous studies, several variables have been identified as having potential relationships with outdoor thermal comfort. However, considering the data availability in each analysis pixel of large-scale urban areas, some relevant parameters were not included. These variables can be categorized into three main categories: (1) Date and time, which can be characterized by the solar zenith angle (SZA) and solar azimuth angle (SAA); (2) Location and morphology, which includes variables such as latitude, longitude, sky view factor (SVF), building density (BD), building height (BH), percentage of green space in the surroundings (P_{green}), percentage of impervious land in the surroundings ($P_{\text{impervious}}$), distance to green space (D_{green}), and distance to waterbody (D_{water}); and (3) Climate, which includes three variables, i.e., air temperature (T_a), relative humidity (rH), and wind speed (V_a). It is important to note that due to the unavailability of globe temperature across large-scale urban areas, we included only the three key meteorological parameters that are accessible during both field studies and large-scale analyses. Overall, a total of 15 potential parameters have been calcu-

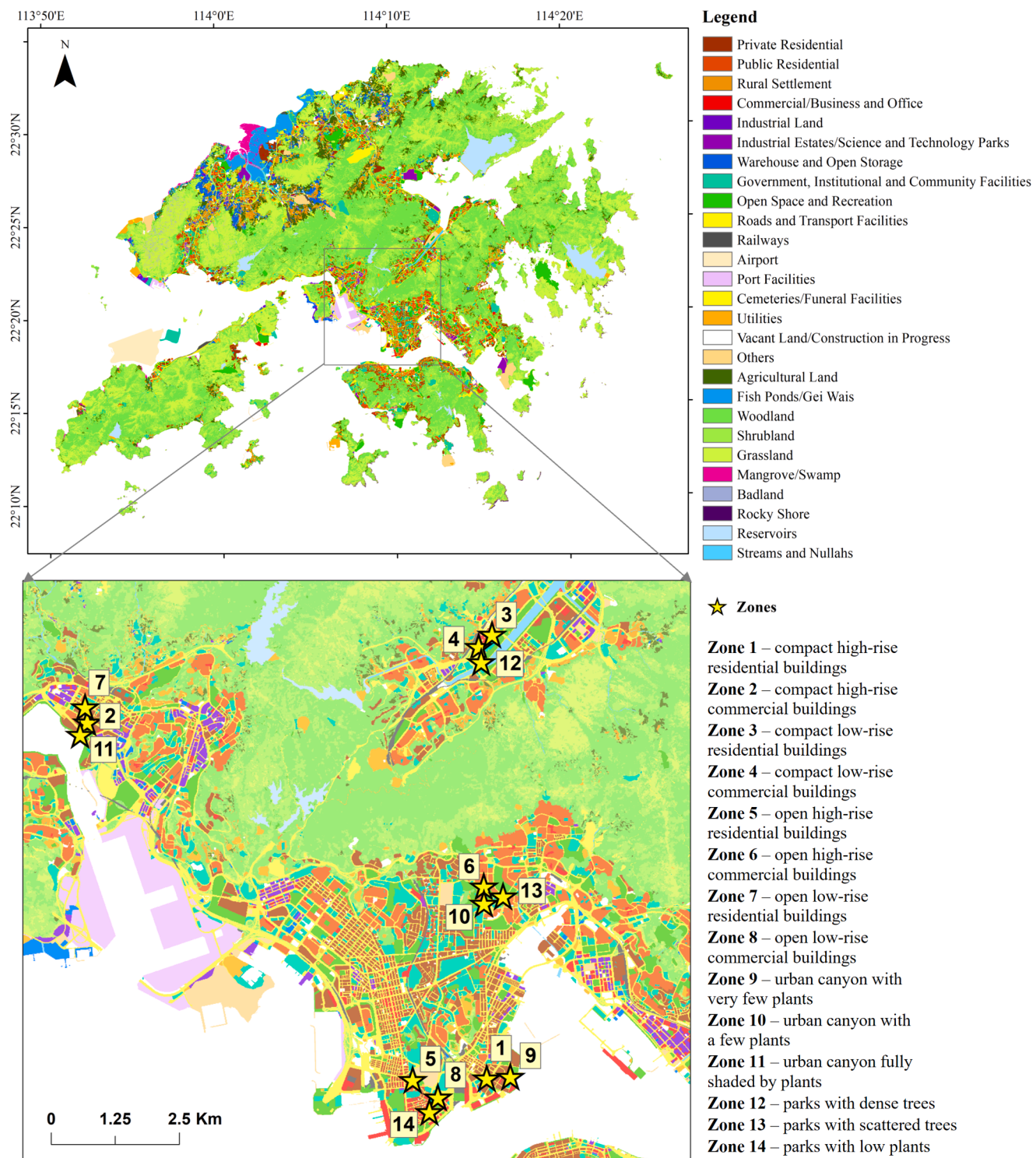


Fig. 2. Study area: Hong Kong.

lated and used as explanatory variables in the predictive models for outdoor thermal comfort (see Fig. 3 for the list of variables).

SZA and SAA were estimated based on the coordinates (latitude, longitude) of the measurement sites and the date and time of the observations. Regarding the morphological parameters, most of the parameters (such as SVF, BD, P_{green} , $P_{impervious}$, D_{green} , and D_{water}) were calculated as percentages based on the objectives present within the entire pixel area ($100\text{ m} \times 100\text{ m}$). BH refers to the average building height within the pixel area (Xu et al., 2017). It is important to note that

when calculating D_{green} and D_{water} , only large water bodies and green spaces with an area larger than 0.1 ha were considered (Aram et al., 2019). Except SVF, all other morphological parameters were calculated using ArcGIS 10.6 software. SVF, which quantifies the proportion of radiation received by a flat surface from the sky in comparison to the total radiation received from the entire hemispheric radiating environment, was calculated using SAGA GIS software (Conrad et al., 2015).

Elevation information was obtained directly from the digital elevation model (DEM) with a 5-m resolution. Building and road coverage

Table 1

The measurement ranges for each sensor.

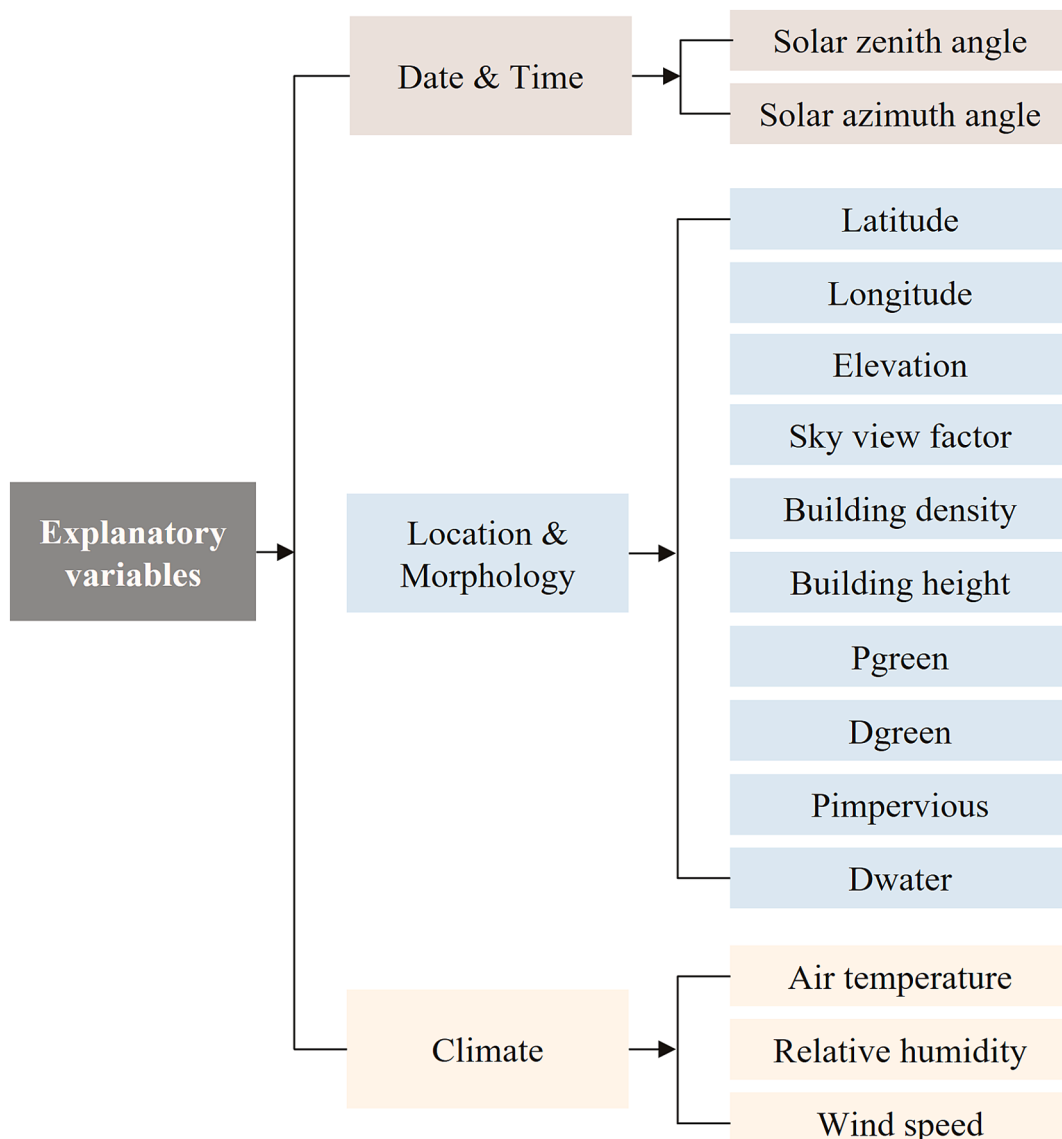
Sensors	Measurement	Specification range	Accuracy
Net radiometer (Kipp & Zonen CNR4)	Short-wave radiation, Long-wave radiation	0.3 to 2.8 μm 4.5 to 42 μm	< 1 % < 1 %
Weather station (Kestrel 5400)	Globe temperature Relative humidity Air temperature Wind speed	-29 to 70 $^{\circ}\text{C}$ 10 to 90 % -29 to 70 $^{\circ}\text{C}$ 0 to 40 m/s	< 1.4 $^{\circ}\text{C}$ < 2 % of reading < 0.5 $^{\circ}\text{C}$ < 20 ft/min

data were derived from the OpenStreetMap (OSM) map. A 5-m resolution DSM is available in Hong Kong, which was generated from the Hong Kong LiDAR Survey. The DSM was used for the calculation of building height data and SVF. To identify green spaces and water bodies, a supervised classification technique and maximum likelihood algorithm were employed to classify Sentinel-2 satellite images (10 m spatial resolution) (Jia & Wang, 2020). Meteorological parameters were collected

using an onsite weather station at the measurement sites, while the GEOS Forward Processing (FP) data product (Lucchesi, 2013) was utilized to collect meteorological parameters for each pixel across the entire urban area.

2.4.2. Computation of thermal comfort indices

A wide range of thermal comfort indices have been utilized to describe human thermal comfort levels, such as the Predicted Mean Vote (PMV) (Fanger, 1970), Standard Effective Temperature (SET*) (Gagge, 1971), Physiological Equivalent Temperature (PET) (Höppe, 1999), and Universal Thermal Climate Index (UTCI) (Blażejczyk et al., 2013). In this study, two commonly-used thermal comfort indices were calculated and compared: PET and UTCI. PET assesses complex outdoor climates by translating them into an indoor scenario based on the Munich Energy-Balance Model for Individuals (MEMI) and the Klima-Michel Model, identifying perceived temperature as an equivalent value (Höppe, 1999; Jendritzky et al., 2000; Staiger et al., 2012). In contrast, UTCI defines the air temperature of a reference environment that results in the same strain index value, based on a given combination of wind, radiation, humidity, and air temperature (Brode et al., 2012). Then, the values from both indices correspond to thermal sensations or stress levels,

**Fig. 3.** The explanatory factors.

represented on PET's nine-level and UTCI's ten-level scales (see Table 2). PET and UTCI have been widely utilized across various climatic conditions (Cheung & Jim, 2018; Pantavou et al., 2018; Wei et al., 2022). In this study, PET was calculated using RayMan 1.2, while UTCI was calculated via the outdoor comfort component in Ladybug for Grasshopper (https://docs.ladybug.tools/ladybug-primer/components/1_analyzedata/utci_comfort).

The calculation of thermal comfort indices requires the inputs of four key meteorological parameters (i.e., T_a , T_{mrt} , rH , and V_a). The integral radiation measurement was used in T_{mrt} calculation. In this method, the mean radiant flux density (S_{str}) of a human body is firstly calculated by multiplying the six individual measurements of the short-wave and long-wave radiant fluxes with the corresponding weights, namely the view factors between a person and the surrounding surfaces. T_{mrt} is then assessed based on Stefan-Boltzmann law from S_{str} . The detailed description of the integral radiation measurement can be found in previous studies (Höppe, 1992; Lai et al., 2017). The calculation procedure of T_{mrt} using the integral radiation measurement can be found in Supplementary Note 2.

2.4.3. Predictive models

The multilayer perceptron (MLP) model, a widely used artificial neural network (ANN) model, was utilized in this study to predict outdoor thermal comfort. The MLP model has demonstrated its effectiveness in predicting the thermal environment in various settings, including both indoor and outdoor conditions (Ketterer & Matzarakis, 2016; Martínez-Comeañá et al., 2021; Yuce et al., 2014). Its structure consists of neurons organized in layers, which starts with an input layer followed by a hidden layer and output later. The connections between these layers are based on a weight structure whose values are altered through model training by using the training dataset. This dataset includes data from 468 sites, which represents 70 % of all data collected through field studies. The remaining 30 % of the dataset, which includes 200 sites, is used to test the model. Following this process, the MLP model structure and the thermal comfort index with the highest predictive accuracy were selected and subsequently applied to broader urban areas and diverse climatic conditions in Hong Kong.

Table 2
Assessment scales of the PET and UTCI.

Class	Description		Range of UTCI (°C)	Range of PET (°C)
	Thermal stress	Thermal sensation		
-5	Extreme cold stress	Very cold	<-40	<4
-4	Very strong cold stress		-40 to -27	
-3	Strong cold stress	Cold	-27 to -13	4-8
-2	Moderate cold stress	Cool	-13 to 0	8-13
-1	Slight cold stress	Slightly cool	0 to +9	13-18
0	No thermal stress	Neutral (comfortable)	+9 to +26	18-23
+1	Slight heat stress	Slightly warm		23-29
+2	Moderate heat stress	Warm	+26 to +32	29-35
+3	Strong heat stress	Hot	+32 to +38	35-41
+4	Very strong heat stress		+38 to +46	
+5	Extreme heat stress	Very hot	>+46	>41

Note: This table was revised from Table 7a and b in the reference (Cheung & Jim, 2018).

3. Results

3.1. Model accuracy

The multilayer perceptron ANN model was used to predict two thermal comfort indices – PET and UTCI – across different datasets. As shown in Fig. 4, the MLP structure demonstrated accurate estimations for outdoor thermal comfort, with R^2 values of 0.90 and 0.95 in the full dataset for PET and UTCI predictions, respectively. Notably, the multilayer perceptron ANN model performed better for the UTCI index (Fig. 4 (d-f)) compared to the prediction of PET index (Fig. 4(a-c)), reaching an R^2 of 0.99 in the training dataset (Fig. 4(e)).

Then, the chosen multilayer perceptron ANN architecture was applied to predict the thermal comfort over the entire urban area of Hong Kong, which comprised a total of 48,381 pixels with a resolution of 100 m. UTCI was applied to represent the daytime outdoor thermal comfort in the following analysis. The climatic conditions for model application include one hot condition and one cold condition in Hong Kong. According to the Hong Kong Observatory, it was recorded the hottest day of 2021 on 23 May, with a maximum air temperature reaching 36.1 °C, while the lowest temperature was 7.7 °C on 8 January.

3.2. Effect of urban morphology on the daytime outdoor thermal environment

The relationship between urban morphology and thermal-related indices (i.e., T_a , T_{mrt} , V_a , and rH) was investigated at the measurement sites. The correlation results are presented in Table 3, providing insights into the associations between these variables.

Among the eight variables, sky view factor (SVF) was found to have the most significant impact on the daytime outdoor thermal environment. The results show significant correlation indices between SVF and ambient temperature (T_a), mean radiant temperature (T_{mrt}), and humidity (rH). The positive correlation observed indicates that as SVF increases, higher temperature and thermal stress can be observed. Following SVF, a strong relationship was also observed between elevation and the thermal indices. Additionally, variables such as impervious surface ratio ($P_{impervious}$), distance to water bodies (D_{water}), and building height (BH) can also affect the outdoor thermal environment. The results reveal that in high-density urban areas of the study region, urban morphology plays a vital role in the daytime thermal conditions. The next section investigates the spatial patterns of daytime outdoor thermal comfort in different urban densities and layouts during varying climates.

3.3. Daytime outdoor thermal comfort in urban spaces of Hong Kong

Fig. 5 illustrates the daytime outdoor thermal comfort across Hong Kong's urban spaces. During extreme hot conditions (Fig. 5(a)), about 74.75 % of urban areas experienced at least strong heat stress, with thermal sensations classified as hot or very hot (UTCI > 32°C). The remaining 25.25 % of areas faced moderate heat stress, with a UTCI between 26 °C and 32 °C. In contrast, during relatively cold conditions (Fig. 5(b)), 40.67 % of urban areas presented no thermal stress (26 °C > UTCI > 9 °C), whereas the majority, at 54.96 %, experienced slight cold stress (9 °C > UTCI > 0 °C). Notably, there were no urban areas in Hong Kong that perceive strong cold stress, even during this coldest condition.

During hot conditions in Hong Kong, strong to extreme heat stress was observed in various locations, including Kowloon Peninsula, Kowloon Bay, Kwai Tsing, the northern region of Hong Kong Island, Tseung Kwan O, and large parts of the New Territories, such as Tin Shui Wai, Tuen Mun, Sheung Shui, Tai Po, and Sha Tin. Conversely, during cold conditions, neutral thermal sensations were prevalent across the New Territories. Notably, in northern Hong Kong, particularly in Sheung Shui and areas adjacent to Shenzhen, some locations even experienced moderate heat stress. To further investigate the spatial patterns of daytime outdoor thermal comfort, we analyzed the distributions of UTCI

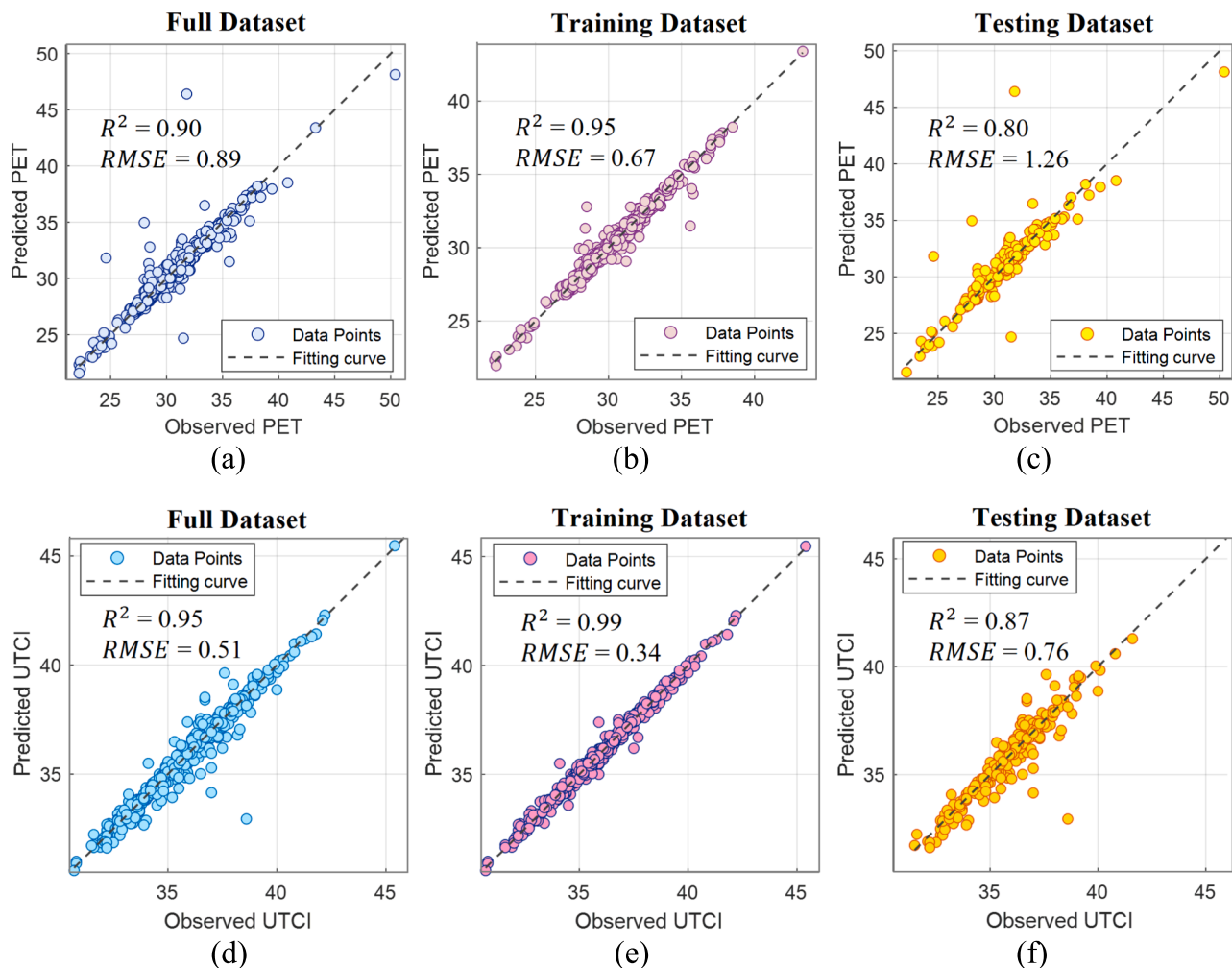


Fig. 4. The multilayer perceptron model accuracy among different datasets for predicting thermal comfort indices: (a) full dataset for PET prediction; (b) training dataset for PET prediction; (c) testing dataset for PET prediction; (d) full dataset for UTCI prediction; (e) training dataset for UTCI prediction; (f) testing dataset for UTCI prediction.

Table 3
Correlations between urban morphological parameters and thermal indices.

Variables	Air temperature (T_a)	Mean radiant temperature (T_{mrt})	Wind speed (V_a)	Relative humidity (rH)
Elevation	0.141**	0.246**	0.055	0.149**
SVF	0.289**	0.589**	-0.041	0.287**
BD	0.003	0.058	-0.048	0.000
BH	-0.040	0.089*	-0.067	-0.036
P _{green}	-0.006	-0.069	-0.044	0.000
P _{impervious}	0.068	0.104*	-0.086*	0.071
D _{green}	-0.033	0.029	0.007	-0.038
D _{water}	0.092*	0.104*	0.078*	0.101**

**. Correlation is significant at the 0.01 level (2-tailed).

*. Correlation is significant at the 0.05 level (2-tailed).

classes based on the predictions of daytime outdoor thermal comfort on the hottest day of the year. Fig. 6 shows the distributions of UTCI classes across six built-up LCZs and 18 administrative districts in Hong Kong.

For the UTCI distribution in built-up LCZs shown in Fig. 6(a), high levels of thermal stress were observed in urban layouts of low-rise buildings. Notably, LCZ 3 exhibited the highest percentage of extreme heat stress (UTCI class = 5), at 61.33 %. LCZ 6 followed closely with a percentage of 57.57 %. In both LCZs 3 and 6, over 90 % of areas experienced strong to extreme thermal stress (UTCI classes = 3, 4, or 5). In

contrast, LCZ 1, characterized by compact high-rise buildings, showed the lowest percentage of high thermal stress, with only 38.13 % of areas experiencing strong to extreme thermal stress.

For the UTCI distribution across administrative districts, as depicted in Fig. 6(b), the North district recorded the highest percentage of extreme heat stress (UTCI class = 5), reaching 98.95 %. In districts such as Tai Po, Yuen Long, and Tuen Mun, the percentages of strong to extreme heat stress (UTCI classes = 3, 4, or 5) were all above 95 %. Meanwhile, districts like Yau Tsim Mong, Tsuen Wan, Sha Tin, and Kowloon City also reported high percentages of strong thermal stress, exceeding 70 %. Conversely, the Eastern district had the lowest percentage of high UTCI values (UTCI > 32°C; UTCI classes = 3, 4, or 5), at 8.80 %.

4. Discussion

4.1. Accuracy of the thermal comfort predictive model in different locations

As illustrated in Fig. 4, the R-squared value for UTCI prediction reached 0.99 in the training dataset (Fig. 4(e)), while the testing dataset also demonstrated a strong R-squared value of 0.87 (Fig. 4(f)). In this section, we further analyzed the relationship between urban morphological parameters, elevation and P_{impervious} showed significant correlations

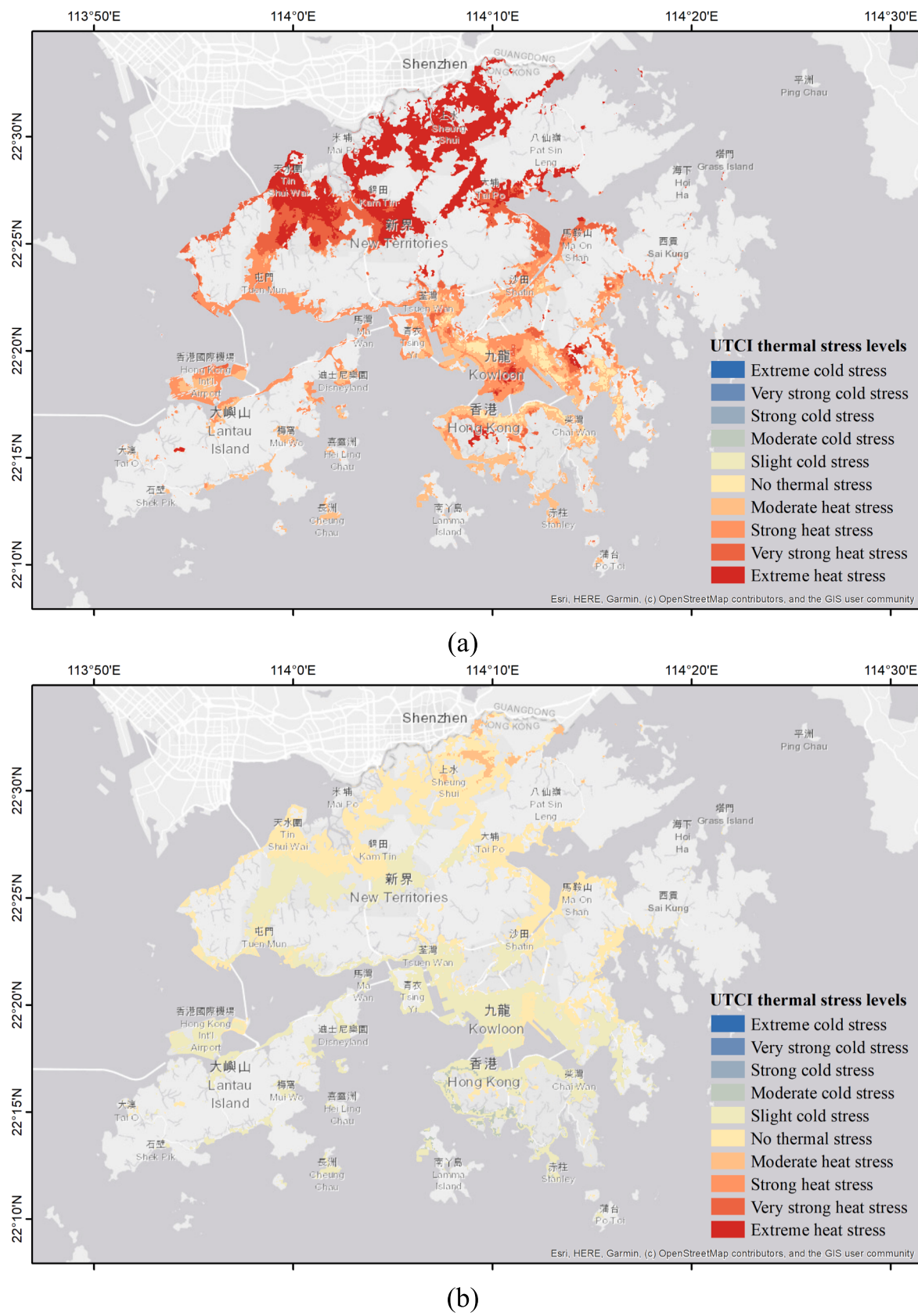


Fig. 5. Daytime outdoor thermal comfort across urban spaces in Hong Kong based on UTCI: (a) on the hottest day of the year; (b) on the coldest day of the year.

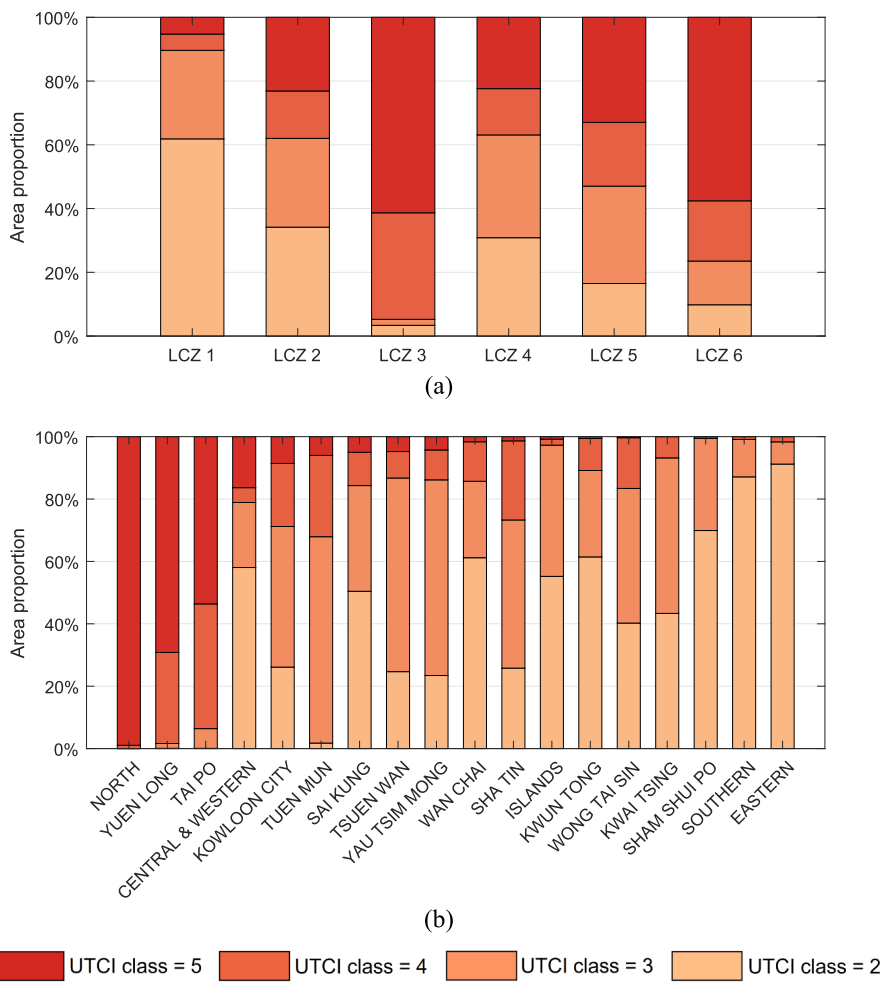


Fig. 6. Distributions of outdoor thermal comfort: (a) in each of six built-up LCZs; (b) in each of the 18 districts in Hong Kong. Note: in (a), LCZ 1 represents compact high-rise built type; LCZ 2 represents compact mid-rise built type; LCZ 3 represents compact low-rise built type; LCZ 4 represents open high-rise built type; LCZ 5 represents open mid-rise built type; and LCZ 6 represents open low-rise built type.

with the model errors. Fig. 7 displays the impacts of these two parameters on the model errors.

As indicated in Fig. 7, model errors were more pronounced in areas with higher elevation and a greater percentage of impervious surfaces. This is primarily due to the strong and dynamic wind conditions in these

regions, which significantly affect model performance. Additionally, open areas experience increased sun exposure, which plays a critical role in outdoor thermal comfort and leads to variations in thermal comfort prediction results. Through the comparison of the impacts of elevation and impervious surfaces on model errors, a more substantial impact of

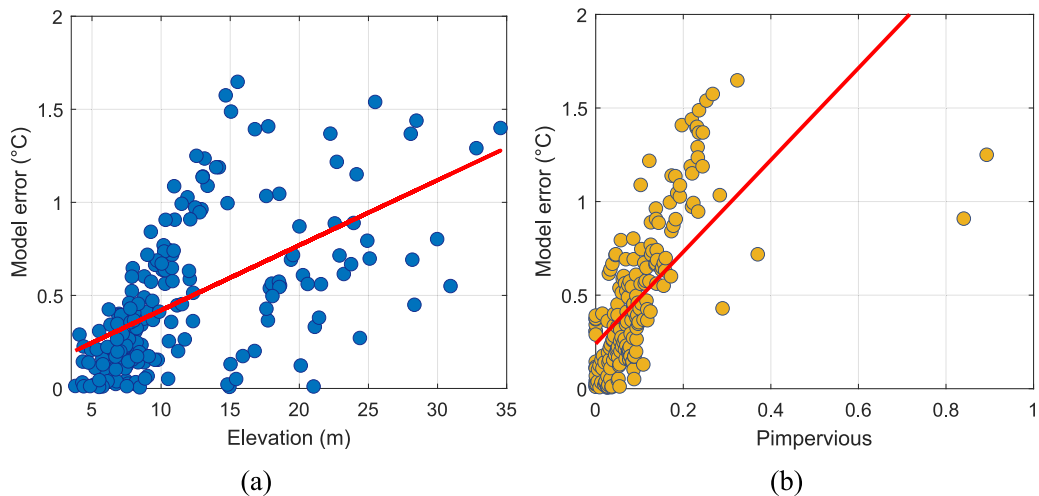


Fig. 7. The relationship between model errors and urban morphology: (a) the impacts of elevation on model errors; (b) the impacts of $P_{\text{impervious}}$ on model errors.

Pimpervious than that of wind can be observed, which was supported by the steeper slope depicted in Fig. 7(b). This aligns with previous findings that temperature and sunlight are the most significant meteorological factors influencing thermal comfort in outdoor spaces (Liu et al., 2022; Xie et al., 2018). Overall, the model demonstrates good performance across a variety of urban areas, particularly in flat and shaded urban environments. While the model has the potential for application in cities with similar climatic and geographical conditions, it should be noted that when applying the proposed framework to regions with distinct climates and urban environments, it is crucial to collect a sufficient number of measurements for re-training the neural network model to ensure accurate large-scale predictions.

4.2. Approaches for enhancing outdoor thermal comfort in wide urban areas

Table 3 indicates the complex interplay of morphological factors that contribute to thermal stress or discomfort. Although there is a positive relationship between SVF and outdoor thermal comfort, indicating the significance of shading in reducing thermal discomfort, in high-density areas such as LCZs 1 to 3, where buildings provide sufficient shading, the extensive use of construction materials and impervious surfaces resulted in high thermal stress. This explains the high percentage of strong heat stress observed in LCZ 3 (as indicated in Fig. 6(a)); as well as the CBD of Hong Kong, e.g., Yau Tsim Mong (see Fig. 6(b)). Conversely, in residential zones like North, Yuen Long, Tai Po, and Tuen Mun, primarily covered by LCZs 4–6, the open building layout allows more sunlight to reach the ground, leading to an increased thermal stress.

These findings also underscore the importance of incorporating nature-based solutions (NBS) for the provision of shading in urban areas. To further evaluate the effectiveness of typical NBS in enhancing outdoor thermal comfort, this study identified and implemented four typical strategies across various urban areas in Hong Kong. These strategies include: (1) green façade, (2) green roof, (3) ground-level grass, and (4) street tree. To model the impact of these strategies on daytime thermal comfort in surrounding outdoor spaces, several widely distributed test sites were selected, with careful modeling of the surrounding environment for each site. ENVI-met, a micro-scale Computational Fluid Dynamics (CFD) model, was used for the scenario development. **Supplementary Note 3** provides more details about the scenario designs of each strategy and implementations of these mitigation strategies in urban areas of Hong Kong. Fig. 8 shows the UTCI reductions by each of the four mitigation strategies in different urban layouts characterized by the built-up LCZs. The simulation results displayed are at 16:00 during the extreme hot condition, the time at which the UTCI in the reference scenario is at its peak.

The simulation results highlight the significant role of street trees in enhancing outdoor thermal comfort, as they can lead to UTCI reductions of up to 4.4 °C in LCZ 6. However, it is challenging to implement ground-level urban green spaces in large-scale outdoor spaces, particularly in

dense urban environments, e.g., LCZs 1–3. Hence, in this section, we further explored various nature-based approaches to improving outdoor thermal comfort in different urban settings.

In dense urban environments, green roof can be an effective option for improving pedestrian-level outdoor thermal comfort, primarily due to the extensive area of building roofs available for implementation. Notably, our study found that green roofs can achieve significant UTCI reductions, with the highest reductions reaching up to 1.5 °C in LCZ 3 with lower building heights. Previous research has also indicated a correlation between the building height and the effect of green roofs in thermal comfort enhancement (Aboelata, 2021). In general, in dense urban environments, green roofs, especially intensive/semi-intensive ones with a relatively high volume of green spaces and thick growing medium layers (Morakinyo et al., 2017), offer an ideal choice for enhancing outdoor thermal comfort. However, it is essential to consider the local climate, building conditions, and urban morphology when implementing green roofs in realistic scenarios, since these external factors may influence the effectiveness and practical feasibility of green roofs in providing thermal comfort benefits (Jamei et al., 2021; Lee & Jim, 2019). Nevertheless, it is important to note that this study utilized typical designs for green roofs and green facades. For instance, all buildings in the study areas featured green roofs with plant heights of 0.50 m, a leaf area index of 2, and a growing medium depth of 0.2 m. More details can be found in **Supplementary Note 3**. However, existing research indicates that the evaporative cooling potential of the vegetation layer depends upon characteristics of vegetation such as foliage density and leaf thickness (Morakinyo et al., 2017). Besides, the researchers identified that the thick green surface and substrate layers contribute to a significant reduction in the heat transfer to the air and the buildings (Castleton et al., 2010; Jamei et al., 2021). Therefore, in practical applications, optimal designs of green roofs should be tested to maximize cooling benefits. Additionally, considerations regarding the structural loadings of buildings for applying green roof systems and maintenance requirements for types featuring trees and shrubs should also be addressed (Castleton et al., 2010; Zhang et al., 2012). Several promising approaches for green roof implementation include positioning trees over structural columns to optimize loading efficiency (Townshend, 2007) and selecting local sedum species for their drought tolerance, ease of propagation, and suitability for shallow substrates.

In open environments with ample space for the ground-level green space, street trees have demonstrated significant improvements in outdoor thermal comfort. In open urban layout (LCZ 4–6), trees have all shown substantial UTCI reductions ranging from 3.3 °C to 4.4°C. However, the thermal comfort improvement by grass was not as pronounced. This is due to the thermal comfort benefits provided by green space are primarily achieved through its shading effect (Rahman et al., 2020), which largely depends on green space quantities such as tree height, leaf area index, and canopy density (Hami et al., 2019; Sun et al., 2017). However, the layout of trees can also impact thermal comfort conditions by affecting wind distribution. Previous studies have shown that a rectangular planting pattern with rows of trees placed perpendicular to the wind direction provides the highest improvement in thermal comfort (Abdi et al., 2020). However, it is important to note that certain tree layouts can create low wind regimes in the downstream area, potentially leading to an increase in UTCI (Lai et al., 2023). In this case, increasing the number of smaller green spaces with a mixture of grass lawns and trees may be considered to reduce the hindrance to wind (Rahman et al., 2020). Overall, ground-level green spaces, particularly trees, have a considerable impact on enhancing thermal environment through their shading capabilities. However, the locations and orientations of trees should be carefully considered when planting them in urban areas. By strategically placing trees, it is possible to optimize their thermal benefits of trees with ensuring satisfactory ventilation.

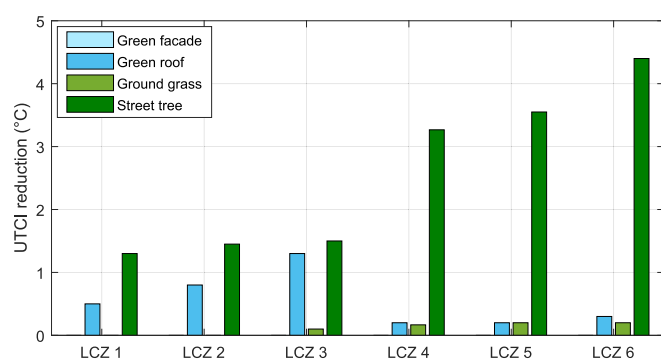


Fig. 8. The UTCI reduction effect by mitigation strategies among built-up LCZs.

5. Conclusions

The paper assessed outdoor thermal comfort in continuous urban areas of Hong Kong coupling onsite measurement and neural network modeling. One key contribution of this research is the development of a systematic framework that integrates micro-scale data collection and macro-scale model employment. The main findings can be summarized below:

- The better multilayer perceptron ANN model performance was observed for the UTCI prediction in wide urban areas compared to that of the PET prediction.
- Urban morphology plays a significant role in outdoor thermal comfort, with the SVF showing the most significant impact on the daytime outdoor thermal environment.
- During the hottest conditions in Hong Kong, there are 74.8 % of areas experiencing strong to extreme heat stress, with thermal sensations classified as hot or very hot, while the remaining 25.3 % fell under moderate heat stress.
- Even during the coldest conditions in Hong Kong, there are 40.7 % of urban areas presenting no thermal stress and 55.0 % of areas experiencing slight cold stress, while no urban areas that perceive strong cold stress.
- High levels of thermal stress were observed in urban layouts of low-rise buildings, with LCZ 3 showing the highest extreme heat stress percentage at 61.3 %, followed by LCZ 6 at 57.6 %. In both LCZs, over 90 % of areas faced strong to extreme thermal stress.

This study contributes to the field of urban planning and design by offering valuable insights into the assessment and improvement of outdoor thermal comfort, particularly in densely populated urban environments like Hong Kong. The findings and methodology can be applied to cities with similar climatic and geographical contexts, facilitating tailored decision-making and effective measures to enhance the outdoor thermal environment. However, as previously discussed, applying the model in regions with distinct climates and urban structures requires further model testing based on field surveys, while strategies for enhancing outdoor thermal comfort may also vary by location. Future research may consider enhancing model performance through three main approaches. First, due to the lack of hourly input data, the current model is unable to predict diurnal patterns of outdoor thermal comfort. To address this, conducting consistent onsite meteorological surveys and incorporating the observations into the model will be beneficial for expanding the temporal scale of the model. Second, integrating advanced remote sensing techniques can effectively improve the model accuracy. For instance, the GEOS Forward Processing (FP) data product was used in this study to provide meteorological parameters for extensive urban areas, while its resolution is limited. By combining advanced deep learning methodologies to downscale satellite product resolution, model accuracy can be enhanced. Third, incorporating additional variables that may affect outdoor thermal environment, e.g., globe temperature, solar radiation, locations of anthropogenic heat sources, green space canopy density, building shapes and orientations, will further refine predictions. Overall, to expand the application of the framework to diverse geographical regions and further improve model performance, future studies should include continuous field research across a variety of climates and urban settings while considering a wider range of inputs.

CRediT authorship contribution statement

Siqi Jia: Writing – original draft, Visualization, Validation, Software, Resources, Methodology, Investigation, Formal analysis, Data curation, Conceptualization. **Yuhong Wang:** Writing – review & editing, Investigation, Data curation. **Nyuk Hien Wong:** Writing – review & editing, Methodology, Investigation, Conceptualization. **Qihao Weng:** Writing –

review & editing, Supervision, Resources, Project administration, Methodology, Funding acquisition, Conceptualization.

Declaration of competing interest

The authors declare that they have no known competing financial interests or personal relationships that could have appeared to influence the work reported in this paper.

Acknowledgements

This work was supported by the Research Talent Hub of the Innovation and Technology Fund and the Global STEM Professorship, both provided by the Hong Kong Special Administrative Region Government.

Appendix A. Supplementary data

Supplementary data to this article can be found online at <https://doi.org/10.1016/j.landurbplan.2024.105281>.

Data availability

Data will be made available on request.

References

- Abdi, B., Hami, A., & Zarehagh, D. (2020). Impact of small-scale tree planting patterns on outdoor cooling and thermal comfort. *Sustainable Cities and Society*, 56. <https://doi.org/10.1016/j.scs.2020.102085>
- Aboelata, A. (2021). Assessment of green roof benefits on buildings' energy-saving by cooling outdoor spaces in different urban densities in arid cities. *Energy*, 219. <https://doi.org/10.1016/j.energy.2020.119514>
- Aram, F., Higueras Garcia, E., Solgi, E., & Mansournia, S. (2019). Urban green space cooling effect in cities. *Heliyon*, 5(4), Article e01339. <https://doi.org/10.1016/j.heliyon.2019.e01339>
- Avashia, V., Garg, A., & Dholakia, H. (2021). Understanding temperature related health risk in context of urban land use changes. *Landscape and Urban Planning*, 212, Article 104107.
- Banfi, A., Tatti, A., Ferrando, M., Fustinoni, D., Zanghirella, F., & Causone, F. (2022). An experimental technique based on globe thermometers for the measurement of mean radiant temperature in urban settings. *Building and Environment*, 222. <https://doi.org/10.1016/j.buldev.2022.109373>
- Bechtel, B., Alexander, P., Böhner, J., Ching, J., Conrad, O., Feddema, J., Mills, G., See, L., & Stewart, I. (2015). Mapping local climate zones for a worldwide database of the form and function of cities. *ISPRS International Journal of Geo-Information*, 4 (1), 199–219. <https://doi.org/10.3390/ijgi4010199>
- Bedford, T., & Warner, C. (1934). The globe thermometer in studies of heating and ventilation. *Epidemiology & Infection*, 34(4), 458–473.
- Blażejczyk, K., Jendritzky, G., Bröde, P., Fiala, D., Havenith, G., Epstein, Y., Psikuta, A., & Kampmann, B. (2013). An introduction to the Universal Thermal Climate Index (UTCI). *Geographia Polonica*, 86(1), 5–10. <https://doi.org/10.7163/GPol.2013.1>
- Bröde, P., Fiala, D., Blażejczyk, K., Holmer, I., Jendritzky, G., Kampmann, B., Tinz, B., & Havenith, G. (2012). Deriving the operational procedure for the Universal Thermal Climate Index (UTCI). *International Journal of Biometeorology*, 56(3), 481–494. <https://doi.org/10.1007/s00484-011-0454-1>
- Castleton, H. F., Stovin, V., Beck, S. B. M., & Davison, J. B. (2010). Green roofs; building energy savings and the potential for retrofit. *Energy and Buildings*, 42(10), 1582–1591. <https://doi.org/10.1016/j.enbuild.2010.05.004>
- Chen, L., & Ng, E. (2012). Outdoor thermal comfort and outdoor activities: A review of research in the past decade. *Cities*, 29(2), 118–125. <https://doi.org/10.1016/j.cities.2011.08.006>
- Cheung, P. K., & Jim, C. Y. (2018). Comparing the cooling effects of a tree and a concrete shelter using PET and UTCI. *Building and Environment*, 130, 49–61. <https://doi.org/10.1016/j.buldev.2017.12.013>
- Conrad, O., Bechtel, B., Bock, M., Dietrich, H., Fischer, E., Gerlitz, L., Wehberg, J., Wichmann, V., & Böhner, J. (2015). System for automated geoscientific analyses (SAGA) v. 2.1. 4. *Geoscientific Model Development Discussions*, 8(2).
- Deng, X., Cao, Q., Wang, L., Wang, W., Wang, S., Wang, S., & Wang, L. (2023). Characterizing urban densification and quantifying its effects on urban thermal environments and human thermal comfort. *Landscape and Urban Planning*, 237, Article 104803.
- Du, J., Sun, C., Liu, L., Chen, X., & Liu, J. (2021). Comparison and modification of measurement and simulation techniques for estimating Tmrt in summer and winter in a severely cold region. *Building and Environment*, 199. <https://doi.org/10.1016/j.buldev.2021.107918>
- Dye, C. (2008). Health and urban living. *Science*, 319(5864), 766–769.
- Fanger, P. O. (1970). Thermal comfort. Analysis and applications in environmental engineering. *Thermal comfort. Analysis and applications in environmental engineering*.

- Gagge, A. P. (1971). An effective temperature scale based on a simple model of human physiological regulatory response. *ASHRAE Transactions*, 77, 247–262.
- Guo, H., Aviv, D., Loyola, M., Teitelbaum, E., Houchois, N., & Meggers, F. (2020). On the understanding of the mean radiant temperature within both the indoor and outdoor environment, a critical review. *Renewable and Sustainable Energy Reviews*, 117. <https://doi.org/10.1016/j.rser.2019.06.014>
- Hami, A., Abdi, B., Zarehagh, D., & Mauan, S. B. (2019). Assessing the thermal comfort effects of green spaces: A systematic review of methods, parameters, and plants' attributes. *Sustainable Cities and Society*, 49. <https://doi.org/10.1016/j.scs.2019.101634>
- Höppe, P. (1992). A new procedure to determine the mean radiant temperature outdoors. *Wetter und Leben*, 44, 147–151.
- Höppe, P. (1999). The physiological equivalent temperature—a universal index for the biometeorological assessment of the thermal environment. *International Journal of Biometeorology*, 43(2), 71–75.
- Huang, J., Zhou, C., Zhuo, Y., Xu, L., & Jiang, Y. (2016). Outdoor thermal environments and activities in open space: An experiment study in humid subtropical climates. *Building and Environment*, 103, 238–249. <https://doi.org/10.1016/j.buildenv.2016.03.029>
- Jamei, E., Chau, H. W., Seyedmohammadi, M., & Stojcevski, A. (2021). Review on the cooling potential of green roofs in different climates. *Science of The Total Environment*, 791, Article 148407. <https://doi.org/10.1016/j.scitotenv.2021.148407>
- Jendritzky, G., Staiger, H., Bucher, K., Grätz, A., & Laschewski, G. (2000). The perceived temperature: The method of the Deutscher Wetterdienst for the assessment of cold stress and heat load for the human body. *Internet workshop on Windchill*.
- Jia, S., & Wang, Y. (2020). Effects of land use and land cover pattern on urban temperature variations: A case study in Hong Kong. *Urban Climate*, 34. <https://doi.org/10.1016/j.ulclim.2020.100693>
- Jia, S., Wang, Y., Wong, N. H., Chen, W., & Ding, X. (2022). Influences of the thermal environment on pedestrians' thermal perception and travel behavior in hot weather. *Building and Environment*, 226. <https://doi.org/10.1016/j.buildenv.2022.109687>
- Johansson, E., Thorsson, S., Emmanuel, R., & Krüger, E. (2014). Instruments and methods in outdoor thermal comfort studies – The need for standardization. *Urban Climate*, 10, 346–366. <https://doi.org/10.1016/j.ulclim.2013.12.002>
- Ketterer, C., & Matzarakis, A. (2016). Mapping the Physiologically Equivalent Temperature in urban areas using artificial neural network. *Landscape and Urban Planning*, 150, 1–9.
- Kumar, P., & Sharma, A. (2020). Study on importance, procedure, and scope of outdoor thermal comfort – A review. *Sustainable Cities and Society*, 61. <https://doi.org/10.1016/j.jscs.2020.102297>
- Lai, A., Maing, M., & Ng, E. (2017). Observational studies of mean radiant temperature across different outdoor spaces under shaded conditions in densely built environment. *Building and Environment*, 114, 397–409. <https://doi.org/10.1016/j.buildenv.2016.12.034>
- Lai, D., Liu, Y., Liao, M., & Yu, B. (2023). Effects of different tree layouts on outdoor thermal comfort of green space in summer Shanghai. *Urban Climate*, 47. <https://doi.org/10.1016/j.ulclim.2022.101398>
- Lau, K.-K.-L., Ren, C., Ho, J., & Ng, E. (2016). Numerical modelling of mean radiant temperature in high-density sub-tropical urban environment. *Energy and Buildings*, 114, 80–86. <https://doi.org/10.1016/j.enbuild.2015.06.035>
- Lau, K.-K.-L., Tan, Z., Morakinyo, T. E., Ren, C., Lau, K.-K.-L., Tan, Z., Morakinyo, T. E., & Ren, C. (2022). Characteristics of Thermal Comfort in Outdoor Environments. In *Outdoor Thermal Comfort in Urban Environment: Assessments and Applications in Urban Planning and Design* (pp. 1–9).
- Lee, L. S. H., & Jim, C. Y. (2019). Urban woodland on intensive green roof improved outdoor thermal comfort in subtropical summer. *International Journal of Biometeorology*, 63(7), 895–909. <https://doi.org/10.1007/s00484-019-01702-4>
- Lindberg, F., Onomura, S., & Grimmond, C. S. B. (2016). Influence of ground surface characteristics on the mean radiant temperature in urban areas. *International Journal of Biometeorology*, 60(9), 1439–1452. <https://doi.org/10.1007/s00484-016-1135-x>
- Liu, K., Lian, Z., Dai, X., & Lai, D. (2022). Comparing the effects of sun and wind on outdoor thermal comfort: A case study based on longitudinal subject tests in cold climate region. *Science of The Total Environment*, 825, Article 154009. <https://doi.org/10.1016/j.scitotenv.2022.154009>
- Liu, K., Nie, T., Liu, W., Liu, Y., & Lai, D. (2020). A machine learning approach to predict outdoor thermal comfort using local skin temperatures. *Sustainable Cities and Society*, 59. <https://doi.org/10.1016/j.jscs.2020.102216>
- Lucchesi, R. (2013). File Specification for GEOS-5 FP. *GMAO Office Note No.*, 4(Version 1.0).
- Manavvi, S., & Rajasekar, E. (2020). Estimating outdoor mean radiant temperature in a humid subtropical climate. *Building and Environment*, 171. <https://doi.org/10.1016/j.buildenv.2020.106658>
- Martínez-Comesaña, M., Ogando-Martínez, A., Troncoso-Pastoriza, F., López-Gómez, J., Febrero-Garrido, L., & Granada-Álvarez, E. (2021). Use of optimised MLP neural networks for spatiotemporal estimation of indoor environmental conditions of existing buildings. *Building and Environment*, 205. <https://doi.org/10.1016/j.buildenv.2021.108243>
- Mayer, H., & Höppe, P. (1987). Thermal comfort of man in different urban environments. *Theoretical and Applied Climatology*, 38(1), 43–49.
- Morakinyo, T. E., Dahanayake, K. W. D. K. C., Ng, E., & Chow, C. L. (2017). Temperature and cooling demand reduction by green-roof types in different climates and urban densities: A co-simulation parametric study. *Energy and Buildings*, 145, 226–237. <https://doi.org/10.1016/j.enbuild.2017.03.066>
- Ng, E., & Cheng, V. (2012). Urban human thermal comfort in hot and humid Hong Kong. *Energy and Buildings*, 55, 51–65. <https://doi.org/10.1016/j.enbuild.2011.09.025>
- Oke, T. R. (1982). The energetic basis of the urban heat island. *Quarterly Journal of the Royal Meteorological Society*, 108(455), 1–24.
- Pantavou, K., Lykoudis, S., Nikolopoulou, M., & Tsilos, I. X. (2018). Thermal sensation and climate: A comparison of UTCI and PET thresholds in different climates. *International Journal of Biometeorology*, 62(9), 1695–1708. <https://doi.org/10.1007/s00484-018-1569-4>
- Plan.Dep. (2019). *Land Utilization in Hong Kong*. Hong Kong University Press.
- Rahman, M. A., Hartmann, C., Moser-Reischl, A., von Strachwitz, M. F., Paeth, H., Pretzsch, H., Pauleit, S., & Rötzer, T. (2020). Tree cooling effects and human thermal comfort under contrasting species and sites. *Agricultural and Forest Meteorology*, 287. <https://doi.org/10.1016/j.agrformet.2020.107947>
- Rossi, F., Cardinali, M., Di Giuseppe, A., Castellani, B., & Nicolini, A. (2022). Outdoor thermal comfort improvement with advanced solar awnings: Subjective and objective survey. *Building and Environment*, 215. <https://doi.org/10.1016/j.buildenv.2022.108967>
- Schweiker, M., Huebner, G. M., Kingma, B. R. M., Kramer, R., & Pallubinsky, H. (2018). Drivers of diversity in human thermal perception - A review for holistic comfort models. *Temperature (Austin)*, 5(4), 308–342. <https://doi.org/10.1080/23328940.2018.1534490>
- Spagnoli, J., & de Dear, R. (2003). A field study of thermal comfort in outdoor and semi-outdoor environments in subtropical Sydney Australia. *Building and Environment*, 38 (5), 721–738. [https://doi.org/10.1016/s0360-1323\(02\)00209-3](https://doi.org/10.1016/s0360-1323(02)00209-3)
- Staiger, H., Laschewski, G., & Grätz, A. (2012). The perceived temperature—a versatile index for the assessment of the human thermal environment. Part A: Scientific basics. *International journal of Biometeorology*, 56, 165–176.
- Stewart, I. D., & Oke, T. R. (2012). Local climate zones for urban temperature studies. *Bulletin of the American Meteorological Society*, 93(12), 1879–1900.
- Su, Y., Wang, C., Li, Z., Meng, Q., Gong, A., Wu, Z., & Zhao, Q. (2024). Summer outdoor thermal comfort assessment in city squares—A case study of cold dry winter, hot summer climate zone. *Sustainable Cities and Society*, 101. <https://doi.org/10.1016/j.jscs.2023.105062>
- Sun, S., Xu, X., Lao, Z., Liu, W., Li, Z., Higueras García, E., He, L., & Zhu, J. (2017). Evaluating the impact of urban green space and landscape design parameters on thermal comfort in hot summer by numerical simulation. *Building and Environment*, 123, 277–288. <https://doi.org/10.1016/j.buildenv.2017.07.010>
- Thorsson, S., Lindberg, F., Eliasson, I., & Holmer, B. (2007). Different methods for estimating the mean radiant temperature in an outdoor urban setting. *International Journal of Climatology*, 27(14), 1983–1993. <https://doi.org/10.1002/joc.1537>
- Townshend, D. (2007). *Study on green roof application in Hong Kong*. Architectural Services Department.
- UNDESA, P. (2018). World urbanization prospects: the 2018 revision. Retrieved August, 26, 2018.
- Vanos, J. K., Rykaczewski, K., Middel, A., Vecellio, D. J., Brown, R. D., & Gillespie, T. J. (2021). Improved methods for estimating mean radiant temperature in hot and sunny outdoor settings. *International Journal of Biometeorology*, 65(6), 967–983. <https://doi.org/10.1007/s00484-021-02131-y>
- VDI. (1998). Methods for the human-biometeorological assessment of climate and air hygiene for urban and regional planning. In: Beuth Berlin.
- Villadiego, K., & Velay-Dabat, M. A. (2014). Outdoor thermal comfort in a hot and humid climate of Colombia: A field study in Barranquilla. *Building and Environment*, 75, 142–152. <https://doi.org/10.1016/j.buildenv.2014.01.017>
- Walikowitz, N., Jänicke, B., Langner, M., Meier, F., & Endlicher, W. (2015). The difference between the mean radiant temperature and the air temperature within indoor environments: A case study during summer conditions. *Building and Environment*, 84, 151–161. <https://doi.org/10.1016/j.buildenv.2014.11.004>
- Wang, R., Ren, C., Xu, Y., Lau, K.-K.-L., & Shi, Y. (2018). Mapping the local climate zones of urban areas by GIS-based and WUDAPT methods: A case study of Hong Kong. *Urban Climate*, 24, 567–576. <https://doi.org/10.1016/j.ulclim.2017.10.001>
- Wei, D., Yang, L., Bao, Z., Lu, Y., & Yang, H. (2022). Variations in outdoor thermal comfort in an urban park in the hot-summer and cold-winter region of China. *Sustainable Cities and Society*, 77. <https://doi.org/10.1016/j.jscs.2021.103535>
- Xie, Y., Huang, T., Li, J., Liu, J., Niu, J., Mak, C. M., & Lin, Z. (2018). Evaluation of a multi-nodal thermal regulation model for assessment of outdoor thermal comfort: Sensitivity to wind speed and solar radiation. *Building and Environment*, 132, 45–56. <https://doi.org/10.1016/j.buildenv.2018.01.025>
- Xu, Y., Ren, C., Ma, P., Ho, J., Wang, W., Lau, K.-K.-L., Lin, H., & Ng, E. (2017). Urban morphology detection and computation for urban climate research. *Landscape and Urban Planning*, 167, 212–224. <https://doi.org/10.1016/j.landurbplan.2017.06.018>
- Yahia, M. W., & Johansson, E. (2014). Landscape interventions in improving thermal comfort in the hot dry city of Damascus, Syria—The example of residential spaces with detached buildings. *Landscape and Urban Planning*, 125, 1–16.
- Yang, W., Wong, N. H., & Jusuf, S. K. (2013). Thermal comfort in outdoor urban spaces in Singapore. *Building and Environment*, 59, 426–435. <https://doi.org/10.1016/j.buildenv.2012.09.008>
- Yin, Q., Cao, Y., & Sun, C. (2021). Research on outdoor thermal comfort of high-density urban center in severe cold area. *Building and Environment*, 200. <https://doi.org/10.1016/j.buildenv.2021.107938>
- Yuce, B., Li, H., Rezgui, Y., Petri, I., Jayan, B., & Yang, C. (2014). Utilizing artificial neural network to predict energy consumption and thermal comfort level: An indoor swimming pool case study. *Energy and Buildings*, 80, 45–56. <https://doi.org/10.1016/j.enbuild.2014.04.052>
- Zhang, X., Shen, L., Tam, V. W. Y., & Lee, W. W. Y. (2012). Barriers to implement extensive green roof systems: A Hong Kong study. *Renewable and Sustainable Energy Reviews*, 16(1), 314–319. <https://doi.org/10.1016/j.rser.2011.07.157>